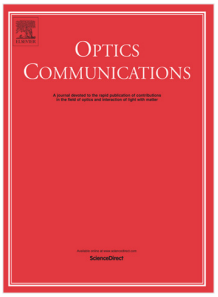

Three-dimensional light sculpting using a geometric analysis

Andrew Bañas, Einstom Engay, Ada-Ioana Bunea, Stephen Daedalus Separa, Jesper Glückstad

PII: S0030-4018(18)30817-4
DOI: https://doi.org/10.1016/j.optcom.2018.09.036
Reference: OPTICS 23475

To appear in: *Optics Communications*

Received date : 17 August 2018
Revised date : 13 September 2018
Accepted date : 15 September 2018

Please cite this article as: A. Bañas, et al., Three-dimensional light sculpting using a geometric analysis, *Optics Communications* (2018), https://doi.org/10.1016/j.optcom.2018.09.036

Three-dimensional light sculpting using a geometric analysis

Andrew Bañas[1,2]*, Einstom Engay[1], Ada-Ioana Bunea[1], Stephen Daedalus Capara[2] and Jesper Glückstad[1,2]

[1]Department of Photonics Engineering, Technical University of Denmark, Ørsted Plads 343, DK-2800 Kgs. Lyngby, Denmark

[2]OptoRobotix ApS, DK-2000 Frederiksberg, Denmark

* Corresponding author: araf@fotonik.dtu.dk

Abstract:

Phase-only spatial light modulators (SLM) have been a staple in laser beam shaping research and applications due to their efficiency and programmability. An SLM's capability to shape three-dimensional distributions of light has interesting applications in optical micromanipulation and microscopy. Since these SLMs operate by modifying the phase of incident light, it is common to model their operation using scalar diffraction theory or Fourier optics. In this work, we show how utilizing a ray tracing or geometric optics analysis can produce both interesting and practical results. We have previously shown how to generate laterally shaped beams that do not have the characteristic noise or discontinuities typical of the output generated with iteratively or numerically derived phase distributions. In this work, we extend the geometric approach to three dimensions to form interesting distributions that behave like non-diffracting beams, light sheets and beams that follow spiraling or diagonal paths as they propagate. The analytically derived input phase functions for these beams can be calculated in a straightforward manner. Hence, they are easily encoded and re-configured for SLM applications. Experiments demonstrate these 3D light distributions on a typical 2*f* holographic configuration, verifying its applicability on existing holographic setups.

Keywords: Laser beam shaping; Digital holography; Fourier optics; Phase-only modulation; Spatial light modulators

1. Introduction

The ability to sculpt light's propagation in three-dimensional space, made possible with programmable spatial light modulators, has many interesting applications. For example, in optical trapping and manipulation, the path traced by the light distribution can be used to direct the trajectory of micro-particles. Airy beams have been used to propel micro-particles along a curved trajectory [1]. Similarly Bessel beams [2,3], known for their extended depth of field have been used to direct particles along a similarly extended path. Vortex beams, known for carrying orbital angular momentum, have been used to revolve particles on a circular path [4], while Helico-Conical beams [5,6] have been used to propel particles along a spiral. Besides such beams that have known analytically formulated input phase functions, or simple custom illumination profiles, there has also been an interest in generating more arbitrary three-dimensional paths with numerically derived phase functions [7]. Beyond spherical particles, custom fabricated micro-particles designed to interact with light differently can lead to even more interesting dynamics [8]. For example, wave-guiding microstructures that bend the direction of light have been shown to follow through optically constructed light rails that are in a direction transverse to the light propagation [9]. A wealth of new applications would therefore be possible if the structural complexities achievable by contemporary microfabrication can be matched by equally complex 3D structures of light.

Besides the ability to spatially control optical force trajectories, 3D sculpted light has also been successfully used for imaging applications. The extended propagation of Bessel [10] or Airy [11] beams has been utilized in microscopy experiments to similarly extend the imaging depth of field. Light sheet

distributions have been used to selectively illuminate planes of a 3D sample [12,13]. Currently, light sheets are commonly implemented using cylindrical lenses [12], or rapidly scanning a beam [14]. Hence, it can be advantageous if such light sheets can be generated dynamically with a programmable spatial light modulator that can simultaneously bring in other new dynamic functionalities into a microscopy experiment, such as optical manipulation, spatially selective stimulation or excitation [15], or aberration correction [16].

1.1. Three dimensional light sculpting using phase-only techniques

In this work, we sculpt light in 3D using an alternative geometric analysis that takes advantage of the rapid re-configurability of phase-only spatial light modulators. We extend the geometric analysis we have used to derive simplified phase functions for extended two-dimensional shapes [17]. The manuscript mainly discusses the light sculpting methodology, while anticipated applications on optical micromanipulation and microscopy would be done on future investigations.

Given the applications of 3D sculpted light, it is inevitable that similar work has been done before. The task at hand is to transform a typical input illumination into the output 3D distributions, preferably through efficient phase-only methods. Although there is a great amount of analytical studies already available [18], it is typical that the final expression for the phase distribution depends on other calculations along the derivations. Occasionally, these previous derivation steps would require integration or solving differential equations, which also implies further numerical steps when translating into a computer implementation. One analytic approach uses the theory of structurally stable coherent and monochromatic beams [19,20] to form continuous distributions such as optical knots or spiral beam paths. Other approaches are conceptually similar to our geometric approach, but instead uses the Eikonal or wave equation [21,22] as the mathematical foundation. It is arguable that these formulations are originally intended for fabricated "fixed" applications such as lenses or freeform optics, wherein there is a pay-off for more involved calculations.

For the experimental use case of encoding phase functions "on-the-fly" on a dynamic SLM, however, one might prefer rapid re-configurability through straightforward calculations, while other figures of merit such as the fidelity or minimal artifacts can be of secondary importance.

In addition to existing mathematical approaches, alternate approaches based on iterative numerical calculations have also been done [23]. Numerical approaches have a minor practical drawback of having to implement an algorithm first. Nevertheless, iterative or numerical methods often have the advantage of generating more arbitrary output distributions. We anticipate utilizing such techniques to further refine or extend our geometric approach. The phase functions derived from such numerical techniques, however, come at the expense of losing a more "intuitive" relation between the input phase and output distribution.

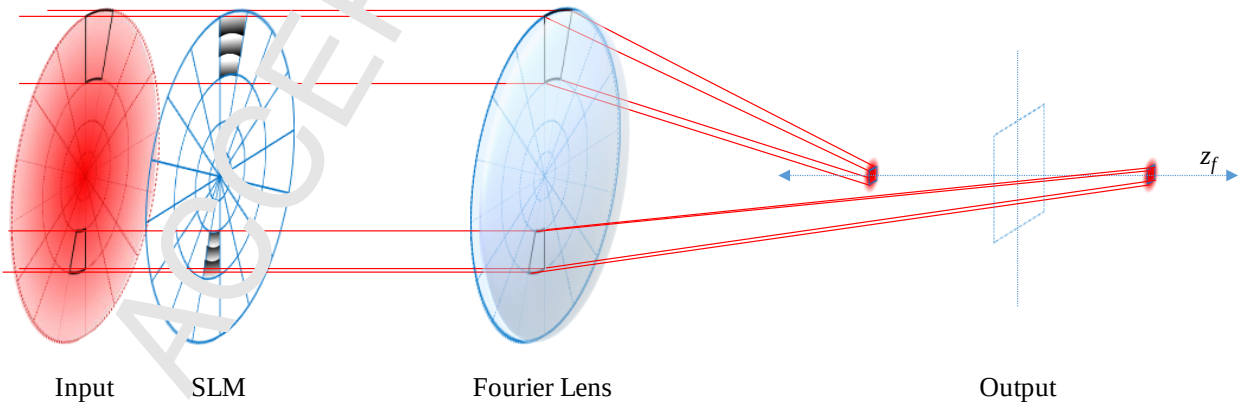

Fig. 1. Conceptual illustration of the geometric mapping approach to laser beam shaping. The input is subdivided such that localized quadratic functions map into different axial locations at the output.

2. Theory

Figure 1 illustrates the conceptual foundation of our method. Using the prism and lens approach, an output focal spot located at (x_f, y_f, z_f) can be generated by Fourier transforming a corresponding analytic expression of the phase input (SLM or phase mask) with coordinates (X, Y).

$$\phi(X,Y;x_f,y_f,z_f) = \frac{2\pi}{\lambda f}\left[\left(X\,x_f + Y\,y_f\right) + \left(X^2+Y^2\right)\frac{z_f}{f}\right] \qquad (1)$$

Here λ is the illumination wavelength and f is the effective focal length of the Fourier transforming lens. For convenience, we normalize axial positions and lengths as a dimensionless fraction of the focal length. In Eqn. 1, the whole input surface is mapped into a single output spot, i.e. (x_f, y_f, z_f) that defines a single coordinate point. One way to extend this input phase to output spot mapping is to randomly divide the input to distinct regions that are to be assigned a corresponding distinct output spot [24]. In this work, instead of mapping the input plane (X, Y) to only one point or distinct separate points, we use a geometric approach that maps local input regions to correspond to a continuous distribution of output coordinates (x_f, y_f). An output shape can thus be defined by a collection of constituent points, (x_f, y_f). This approach has been successful in generating extended 2D shapes wherein continuous adjacent points (x_f, y_f) constitute the output shape [17]. Our geometric mapping thus takes the general form

$$\phi(X,Y) = \frac{2\pi}{\lambda f}\left[X\,x_f(X,Y) + Y\,y_f(X,Y) + \left(X^2+Y^2\right)\frac{z_f(X,Y)}{f}\right] \qquad (2)$$

The first two terms in Eqn. 2 that multiply with x_f and y_f describe the lateral distribution of the output. In some of our examples, we used a line profile as the lateral distribution by encoding a zero-width rectangular point spread function (PSF) [17]. Other known input phase functions that have a direct mapping to the laterally defined output can also be used. For example, we have used a helical phase ramp to map the input light into a ring distribution.

Continuing the analogy with a single point in 3D, (x_f, y_f, z_f) in Eqn. 1, the principle is further extended to the axial dimension by applying a local quadratic or lens function to translate a correspondingly mapped output spot to a specified axial location. Hence, just as we define the lateral output shape as a distribution of x_f and y_f that is dependent on the input coordinates, we can similarly define the localized z_f of subdivisions of the output shape through a similar mapping $z_f(X, Y)$.

The main task in our approach is to identify mapping functions, $x_f(X, Y)$, $y_f(X, Y)$ and now, $z_f(X, Y)$, that can be substituted back into Eqn. 2. It is in this part where we analyze the geometry of the intended distribution, then use energy conservation rules to derive an applicable mapping. In the following sections, we show specific examples of how the geometric mapping principle is utilized to derive corresponding input phase functions.

2.1. Stretched vortex beams

In this example application, we linearly map azimuthal divisions of the input plane into output axial locations between a defined minimum and maximum output z_f coordinate. To formulate, for a given angle, θ, at the input plane the mapped z_f follows the form:

$$z_f(\theta) = C_z\theta \qquad (3)$$

Neglecting the SLM's rectangle boundaries, the input amplitude is assumed to be radially symmetric such that each angular sub-division has the same amount of energy. If we normalize the angle, we will have an expression that depends on the desired propagation length. For calculation convenience, we also express the angle in terms of X and Y (and use the range of the atan2 inverse tangent implementation, $-\pi$ to π).

$$z_f(X,Y) = \frac{L_{zf}}{2\pi}\tan^{-1}\left(\frac{Y}{X}\right) \qquad (4)$$

So far, this only defines the output's axial distribution. To get results that are easier to observe, we should also define how x_f and y_f is to be mapped. Here, we utilize the so-called vortex or Laguerre-Gaussian beam whose phase is defined by $l\theta$, l being the topological charge. The helical phase can also be

interpreted as infinitesimal planar ramps that follow the azimuthal angle. By multiplying the associated quadratic term to the axial mapping and using the vortex phase directly, we arrive at the following expression.

$$\phi(X,Y) = l\tan^{-1}\left(\frac{Y}{X}\right) + \frac{(X^2+Y^2)}{\lambda f}\tan^{-1}\left(\frac{Y}{X}\right)\frac{L_{zf}}{f} \quad (5)$$

We note that as θ approaches the degenerate values, -π and π, there is a discontinuity in the mapped z_f locations, which are the extremes, $-L_{zf}/2$ and $L_{zf}/2$. This discontinuity is evident in the experiment with the usual vortex ring now broken and fading into darkness. A similar beam referred to as a "light sword" has been reported before [25], but without the helical phase ramp contribution (l=0). Without the lateral mapping associated with the vortex ring profile, the light sword has its energy centered at the optical axis, hence, it was proposed for extending the depth of focus in imaging systems. In the next section, we propose an alternative beam that might be more suitable for extended depth of focus application, given its similarities with Bessel beams that have been commonly used for the said application.

2.2. Pseudo Bessel beams

The standard way of implementing Bessel beams is to have a ring shaped illumination or an axicon lens at the input. Additional components and modifications of a typical 2f diffractive focusing setup are thus necessary if one wishes to use Bessel beams on a sample. We demonstrate that by continuously stacking adjacent foci along the optical axis, we can emulate the desired characteristic of Bessel beams which is its extended propagation length where the beam intensity remains localized.

We assume that the input has a Gaussian illumination with 1/e^2 half beam waist, w_0. To derive the input phase function, we then assume that the input energy is evenly spread throughout a line segment along z_f with a length L_{zf} and some constant energy density ρ_{zf}. The following expression then describes the conservation relation for such setup.

$$\pi w_0^2 = \rho_{zf} L_{zf} \quad (6)$$

We assume radial symmetry on the input amplitude such that concentric ring shaped regions at the input are mapped into the succeeding z_f subdivisions. For brevity, we use R, the radial coordinate at the input, as a shorthand for $\sqrt{X^2+Y^2}$. If we impose that a radial segment bounded by R has the same energy as a linear segment bounded by the correspondingly mapped axial position z_f, we arrive at the following conservation rule.

$$\frac{\pi w_0^2\left(1 - e^{-\frac{R^2}{w_0^2}}\right)}{\pi w_0^2} = \frac{\rho_{zf} z_f}{\rho_{zf} L_{zf}} \quad (7)$$

The above expression results to the following input radius to output axial position mapping.

$$z_f(R) = L_{zf}\left(1 - e^{-\frac{R^2}{w_0^2}}\right) \quad (8)$$

This above form is very similar to what we used to generate a circular PSF [17], except that the output is mapped along a line, and hence the coordinate mapping should be multiplied with a quadratic function. Hence, we arrive at the following phase function:

$$\phi(R) = \frac{2\pi}{\lambda f} R^2 \frac{L_{zf}}{f}\left(1 - e^{-\frac{R^2}{w_0^2}}\right) \quad (9)$$

Unlike with the stretched vortex beam, x_f and y_f can be set as zero for this case.

2.3. Light sheets

We define two conditions to generate a light sheet. First, the lateral projection of output has to be stretched in one direction such as x_f or y_f. Second, this stretched profile should have a minimal divergence as it propagates along z_f, just as with the pseudo-Bessel beam. We use a zero-width rectangle to first

define a line distribution along a chosen transverse axis. Choosing X or x_f as the lateral axis, the following phase function forms a line with length L_{xf} at the Fourier plane.

$$\phi(X,Y) = \frac{2\pi}{\lambda f} X\, L_{xf}\, \mathrm{erf}\left(\frac{X}{w_0}\right) \Big/ \mathrm{erf}\left(\frac{A}{w_0}\right) \tag{10}$$

Here, A is the length of the input along the X-axis as defined in [17]. Away the focal plane the x_f-line beam would normally be diverging along the y_f-direction, hence we chose to map input segments along Y into successive z_f segments at the output. Similar to the pseudo-Bessel beam phase derivation, we start by assuming a conservation relation.

$$\int \exp[-(X^2 + Y^2)/w_0^2]\, dY = \rho_{zf} L_{zf} \tag{11}$$

The above integral is separable in X and Y and the result is known to involve the error function. Assuming that the input's rectangular boundaries has the width and height, A and B, we obtain the following expression:

$$\mathrm{erf}\left(\frac{A}{w_0}\right)\mathrm{erf}\left(\frac{Y}{w_0}\right) \Big/ \mathrm{erf}\left(\frac{A}{w_0}\right)\mathrm{erf}\left(\frac{B}{w_0}\right) = \frac{\rho_{zf} z_f}{\rho_{zf} L_{zf}} \tag{12}$$

Solving for z_f, we obtain the following mapping for to the input Y.

$$z_f(Y) = L_{zf}\, \mathrm{erf}\left(\frac{Y}{w_0}\right) \Big/ \mathrm{erf}\left(\frac{B}{w_0}\right) \tag{13}$$

Combining Eqn. 13 and Eqn. 10 into Eqn. 2, we arrive at the following input phase function for a light sheet whose plane lies on the x_f-z_f axis.

$$\phi(X,Y) = \frac{2\pi}{\lambda f}\left[X\, L_{xf}\, \mathrm{erf}\left(\frac{X}{w_0}\right) \Big/ \mathrm{erf}\left(\frac{A}{w_0}\right) + \kappa \frac{L_{zf}}{f}\, \mathrm{erf}\left(\frac{Y}{w_0}\right) \Big/ \mathrm{erf}\left(\frac{B}{w_0}\right)\right] \tag{14}$$

It is interesting to note that if we instead choose to map z_f along the input X-direction, i.e. in the direction of the projected line, we get an output distribution with a peak that traverses a diagonal path as it propagates. The expression is similar to that of the light sheet, however, similar to the stretched helical beam, bilateral symmetric mapping is no longer assumed with one X-end mapping to a closer z_f while the opposite X-end maps to the further z_f.

3. Limitations of our geometric approach

The adherence of our approach to analytically tractable formulations is not without disadvantages. As pointed out, it lacks the arbitrary control of numerical approaches. Furthermore, there is a limited amount of special case output distributions wherein one could derive phase functions that can be directly encoded. Some examples are presented in this work. As our approach uses a direct mapping between input regions and their corresponding output locations, our approach is inherently limited by the finite area of the input (SLM).

3.1. Limiting to laterally confined light distributions

We previously demonstrated the shaping of laterally extended light regions [17]. These shaped beams are an example of continuously controlling the lateral location of the constituent output light regions. Continuous axial control, however, is best demonstrated for beams that are laterally confined, i.e. beams that project spots or line paths at a given lateral plane. In such distributions, it is easier to observe where the given line segments are focused. It should be noted that light directed at a 3D location has to come from somewhere. Hence, unless the destination is relatively focused, the intensity of light propagating before and after that specified location would be at a similar level, decreasing the visibility of the intended output.

3.2. Intended use for light shaping

In previous works [17,26], we defined a distinction between light shaping and light distribution, that allowed us to break down the overall task into simpler methodologies that can be individually optimized.

In light shaping, we transform an individual unit spot into another shape or beam typically contiguous in both phase and amplitude. Light distribution, on the other hand, typically distributes multiple copies of these individually shaped beams, utilizing convolution on top of another phase function intended for arranging the focal spots, or the respective point spread functions, into a collection of distinct output positions. The geometric approach here is best categorized as a light shaping technique, whose output is intended to be multiplexed. Our experiments in the next section only show a single beam and utilize a blazed or planar grating distributing phase to displace the shaped beam away from the zero order.

4. Experiments

4.1. Axially sampled beam propagation

We performed the experiments using a typical 2*f* Fourier transforming SLM setup, but with a long focal length lens to directly project the output to a CCD camera with a sufficient magnification. The holographic setup uses the same components as the one used in [17] with slight modifications to allow systematic collection of snapshots at different axial planes. An 800×600 SLM with a 20µm pitch (Hamamatsu Photonics) is illuminated with a 635nm wavelength laser with a 1/e^2 beam diameter of about 6mm. The Fourier transforming lens has a 350mm focal length while the camera used has a 4.45µm pixel pitch (Point Grey with Sony sensor). The encoded phases are shown on Fig. 2. A blazed grating phase is also superposed on these phase patterns to shift the output away from the zero order, but is excluded from the figure to avoid visually obscuring the directly calculated phase distributions. The zero order is utilized as a convenient visual reference of how much a typical focal spot would be diverging at a given axial plane. Snapshots of different beams are taken at approximately 2cm intervals before and after the focal plane as shown in Fig. 3. All snapshots are aligned using the center of the zero order (which has been cropped out except for the case of the pseudo-Bessel beam). With the exception of the regular vortex and line focus beams used for reference, we chose a confined axial propagation length that is 0.2 times the focal length (~7cm).

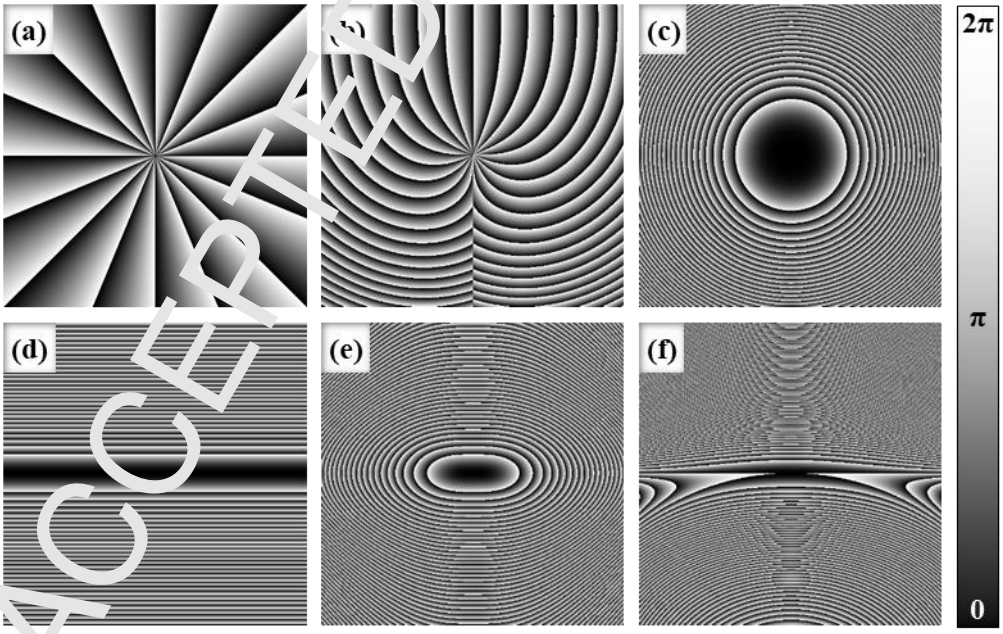

Fig. 2. Phase patterns used for the experimental demonstrations. These are encoded as 800×600px^2 (cropped to 600×600 px^2) on the 16x12mm^2 SLM surface. The phase distributions correspond to the regular (a) and stretched (b) vortex, the pseudo-Bessel beam (c), the line focus (d), the light sheet (e) and the diagonal beam path (f). These plots are rotated for consistency with the experiment's camera orientation.

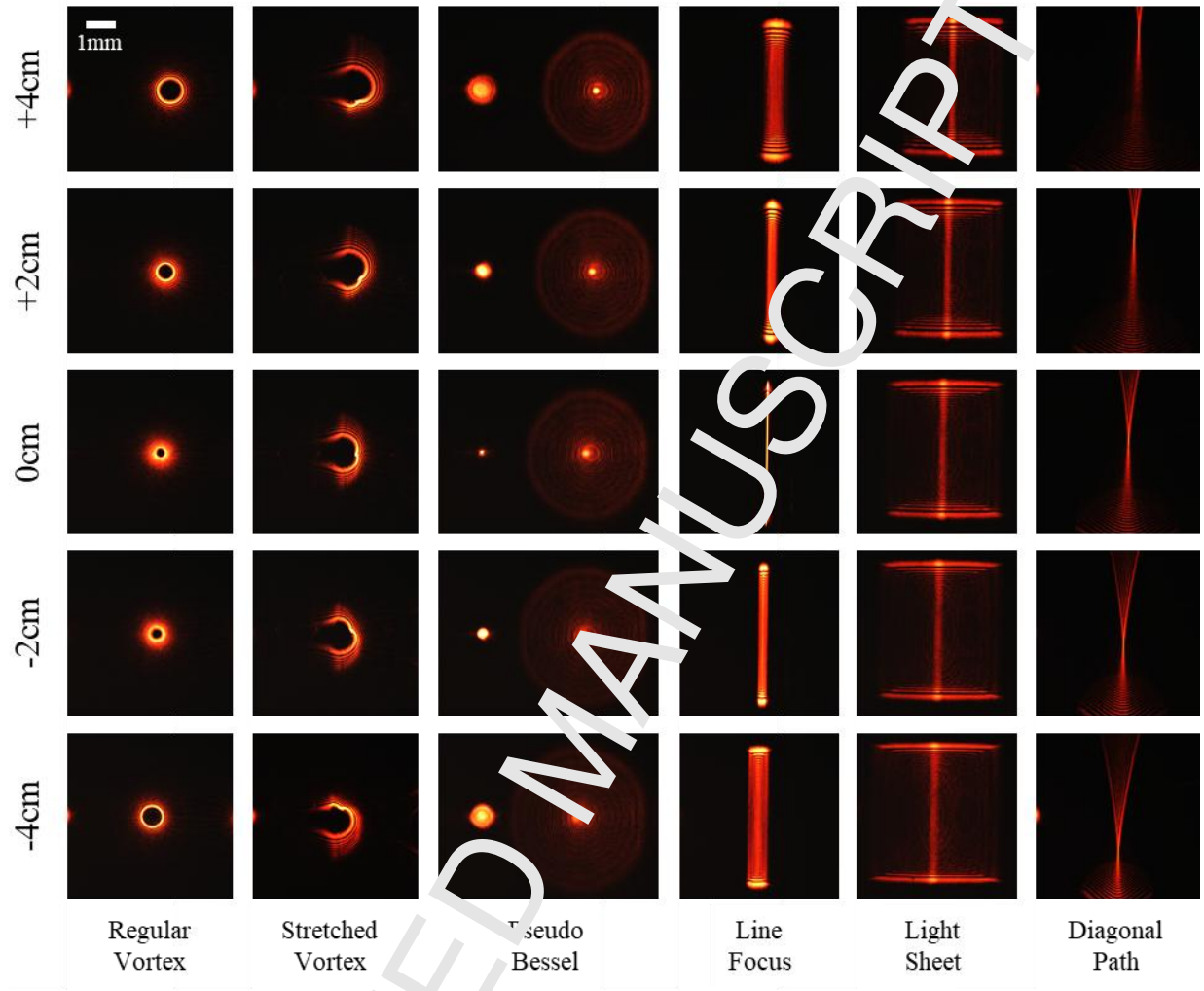

Fig. 3. Snapshots of the different beams taken at different z_f planes, ~2cm apart. The scale bar is 1mm at the CCD. The un-diffracted zero order is shown alongside the pseudo-Bessel beam serving as a reference.

4.1.1. Stretched vortex beam

We used a helical phase with $\ell = 16$ to define the beam's lateral ring distribution. For comparison, a non-stretched "regular" vortex beam with the same topological charge was also captured. With the axial stretching phase applied, there is an observed increase in the vortex's apparent radius. But this could be due to the focus offset of the ring's segments, and the associated beam divergence as the segments are further from the focal plane. Another observation is the existence of a "bump" along the broken ring profile, associated with the ring segment that is in focus at a given camera position.

It is interesting to note that the resulting stretched vortex beam has proven useful for assessing when the camera is closest to the focal plane. The beam associates a prominent lateral feature, the intensity bump, to axial position. The beam profile is most symmetric when at the focal plane. The bump along the broken ring then changes its angular position as the camera moves axially. Compared to typically quantifying the spread or brightness of the beam, which need to be compared to measurements from adjacent z_f-planes, looking for the position of this intense "bump" can be done with only one captured image. With calibration, the angular location of the bump would also be useful for identifying z_f locations other than the focal plane. We anticipate this beam to have practical measurement or calibration uses.

4.1.2. Pseudo Bessel beam, light sheet and diagonal beam

The beams whose SLM phase are described in equations (9) and (14) not only show their non-diffracting behavior, but also, similar to Bessel beams, that they utilize off-focused light from previous planes to form the peak at a given plane. Hence, the peak intensity is lower than that of a diffraction limited focal spot. Furthermore, despite diverging slowly, the beam width is broader. To qualitatively assess the light sheet's diffraction, a line focus, formed by using a rectangular PSF phase [17] with a zero width, is also captured. Analogous to the comparative behavior of the focal spot and pseudo-Bessel beam, the light sheet is also broader at the focal plane, but diverges less compared to the line focus. We also tested the generation of a diagonally traversing beam. The peak's relative vertical location with respect to the zero order can be seen going up as the camera moves further from the focusing lens.

4.2. Side view visualization

In order to get more intuitive visualization of the 3D propagation, side view images of select beam profiles are observed. Fluorescent dye from a marker pen is dissolved in water and loaded into a cuvette with a 250µm channel height (Hellma Analytics). A setup similar to our Biophotonics Workstation [27] is used. This uses long working distance objectives to form the laser path through the fluorescent sample. The long working distance permits enough space to place another objective lens through the side of the sample from which we collected the side view images. A 532nm wavelength laser, also with a ~6mm beam diameter, illuminates an 800×600 SLM with a 20µm pitch (Hamamatsu Photonics). The SLM plane is relayed with a 1/3 magnification to the back aperture of an objective lens that has a 9mm focal length (NA 0.45).

The captured side view fluorescent images are shown in Fig. 4. The un-diffracted zero order can be seen at the left of the encoded beams, and conveniently serves as a reference. A simple displaced first-order spot (a) is also shown, exhibiting the typical waist where the beam is most focused. Compared to the displaced first order beam (a), it can be seen that the pseudo-Bessel beam forms a straighter line, but has a lower brightness and more background peripheral light. The phase pattern of the light sheet beam is encoded at two orientations to provide a perpendicular (c) and parallel (d) view to the plane of the light sheet. Viewed through its narrower side, the light sheet looks nearly identical to the pseudo-Bessel beam.

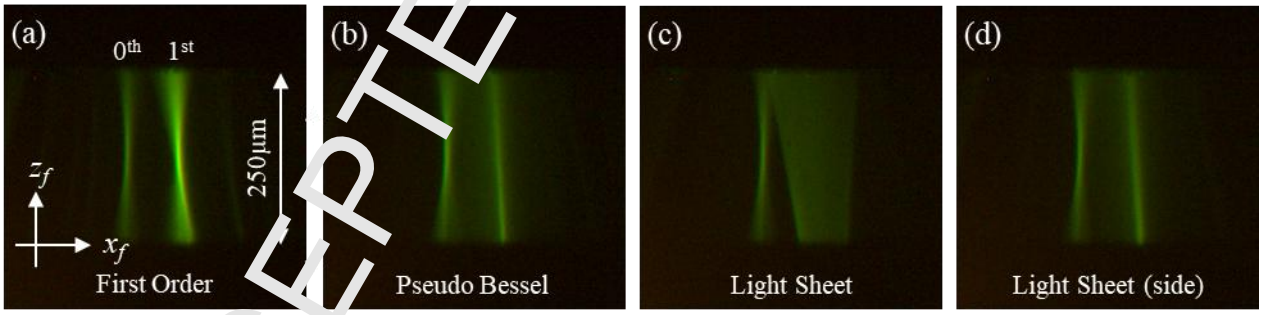

Fig. 4. Side view images of a diffraction-limited, displaced first-order spot (a), pseudo-Bessel beam (b) and perpendicular light sheets (c) and (d), going through a fluorescent sample. The un-diffracted zero order can be seen on the left of each beam, serving as a reference.

5. Conclusions

This work presents a new approach of shaping 3D laser distributions in focusing systems. Compared to what has been done before, this approach utilizes geometric optics as the underlying theory while utilizing deterministic phase distributions used in diffractive optics to implement the geometric mapping. Despite the approximate nature, the derived phase functions have the advantage of being "stand alone", hence being straightforward to implement and tune in live experiments. From this principle, we were able to derive phase functions for beams that can be used for axial calibration and beams that exhibit the extended depth of field of Bessel beams and light sheets. From a practical standpoint, this means that we

can approximate the qualities of Bessel beams and light sheets without the need of an axicon or cylindrical lens elements, provided an SLM is available. These phase distributions thus extend the functionality of existing setups for computer-generated holography. Future work shall study the individual beam cases in detail as this work mainly focused on the general methodology for generating this class of beams. It would also be interesting to investigate numerical techniques that might supplement the analytic approach presented here.

Acknowledgements

This work has been supported by the Lundbeck Foundation (Grant number R244-2016-3941), the Novo Nordisk Foundation (Grand Challenge Program; NNF16OC0021948) the Combined Molecular Microscopy for Therapy and Personalized Medication in Rare Anaemia Treatments (CoMMiTMent) FP7 collaborative project (Grant agreement number: 602121), and the Regulation of red cell life-span, erythropoiesis, survival, senescence and clearance (Project ID 675115) Horizon-2020 training network. We also thank our industrial collaborator, Hamamatsu Photonics K.K. Central Research Laboratory. Many portions of the setup used for fluorescence imaging were built by Manto Chouliara.

References

1. J. Baumgartl, M. Mazilu, and K. Dholakia, "Optically mediated particle clearing using Airy wavepackets," Nat. Photonics **2**, 675 (2008).
2. T. Čižmár, V. Garcés-Chávez, K. Dholakia, and P. Zemánek, "Optical conveyor belt for delivery of submicron objects," Appl. Phys. Lett. **86**, 174101 (2005).
3. J. Arlt, V. Garces-Chavez, W. Sibbett, and K. Dholakia, "Optical micromanipulation using a Bessel light beam," Opt. Commun. **197**, 239–245 (2001).
4. J. E. Curtis and D. G. Grier, "Structure of optical vortices," Phys. Rev. Lett. **90**, 133901 (2003).
5. C. A. Alonzo, P. J. Rodrigo, and J. Glückstad, "Helico-conical optical beams: a product of helical and conical phase fronts," Opt. Express **13**, 1749–1760 (2005).
6. V. R. Daria, D. Z. Palima, and J. Glückstad, "Optical twists in phase and amplitude," Opt. Express **19**, 476–81 (2011).
7. M. R. Dennis, R. P. King, B. Jack, K. O'Holleran, and M. J. Padgett, "Isolated optical vortex knots," Nat. Phys. **6**, 118 (2010).
8. J. Glückstad and D. Palima, *Light Robotics-Structure-Mediated Nanobiophotonics* (Elsevier, 2017).
9. D. Palima, A. R. Bañas, G. Vizsnyiczai, L. Kelemen, T. Aabo, P. Ormos, and J. Glückstad, "Optical forces through guided light deflections.," Opt. Express **21**, 581–93 (2013).
10. E. J. Botcherby, R. Juškaitis, and T. Wilson, "Scanning two photon fluorescence microscopy with extended depth of field," Opt. Commun. **268**, 253–260 (2006).
11. D. L. Marks, R. A. Stack, D. J. Brady, and J. van der Gracht, "Three-dimensional tomography using a cubic-phase plate extended depth-of-field system," Opt. Lett. **24**, 253–255 (1999).
12. J. Huisken, J. Swoger, F. Del Bene, J. Wittbrodt, and E. H. K. Stelzer, "Optical Sectioning Deep Inside Live Embryos by Selective Plane Illumination Microscopy," Science (80-.). **305**, 1007–1009 (2004).
13. M. Weber, M. Mickoleit, and J. Huisken, "Chapter 11 - Light sheet microscopy," in *Quantitative Imaging in Cell Biology*, J. C. Waters and T. Wittman, eds., Methods in Cell Biology (Academic Press, 2014), Vol. 123, pp. 193–215.
14. P. J. Keller, F. Pampaloni, and E. H. K. Stelzer, "Life sciences require the third dimension," Curr. Opin. Cell Biol. **18**, 117–124 (2006).
15. E. Papagiakoumou, F. Anselmi, A. Bègue, V. de Sars, J. Glückstad, E. Y. Isacoff, and V. Emiliani, "Scanless two-photon excitation of channelrhodopsin-2.," Nat. Methods **7**, 848–54 (2010).
16. T. Čižmár, M. Mazilu, and K. Dholakia, "In situ wavefront correction and its application to

micromanipulation," Nat. Photonics **4**, 388–394 (2010).
17. A. Bañas, S. D. Separa, E. Engay, and J. Glückstad, "Point spread function shaping using geometric analysis," Opt. Commun. **427**, 522–527 (2018).
18. F. M. Dickey, *Laser Beam Shaping: Theory and Techniques* (CRC press, 2014).
19. E. G. Abramochkin and V. G. Volostnikov, "Spiral light beams," Physics-Uspekhi **47**, 1177–1203 (2004).
20. J. A. Rodrigo, T. Alieva, E. Abramochkin, and I. Castro, "Shaping of light beams along curves in three dimensions," Opt. Express **21**, 20544–20555 (2013).
21. L. L. Doskolovich, A. Y. Dmitriev, and S. I. Kharitonov, "Analytic design of optical elements generating a line focus," Opt. Eng. **52**, 91707 (2013).
22. V. A. Soifer, ed., "Calculation of diffractive optical elements in geometrical optics approximation," in *Computer Design of Diffractive Optics*, Woodhead Publishing Series in Electronic and Optical Materials (Woodhead Publishing, 2013), pp. 92–195.
23. T. Latychevskaia and H.-W. Fink, "Inverted Gabor holography principle for tailoring arbitrary shaped three-dimensional beams," Sci. Rep. **6**, 26312 (2016).
24. M. Montes-Usategui, E. Pleguezuelos, J. Andilla, and E. Martín-Badosa, "Fast generation of holographic optical tweezers by random mask encoding of Fourier components," Opt. Express **14**, 2101–2107 (2006).
25. A. Kołodziejczyk, S. Bará, Z. Jaroszewicz, and M. Sypek, "The Light Sword Optical Element—a New Diffraction Structure with Extended Depth of Focus," J. Mod. Opt. **37**, 1283–1286 (1990).
26. A. Bañas and J. Glückstad, "Holo-GPC: Holographic Generalized Phase Contrast," Opt. Commun. **392**, 190–195 (2017).
27. H.-U. Ulriksen, J. Thogersen, S. Keiding, I. R. Perch-Nielsen, J. S. Dam, D. Z. Palima, H. Stapelfeldt, and J. Glückstad, "Independent trapping, manipulation and characterization by an all-optical biophotonics workstation," J. Eur. Opt. Soc. Rapid Publ. **3**, (2008).